

# Self-Assembly of dPS-Liquid Crystalline Diblock Copolymer in a Nematic Liquid Crystal Solvent

Soo-Young Park,<sup>†,\*</sup> Thangavelu Kavitha,<sup>†</sup> Tahseen Kamal,<sup>†</sup> Waliullah Khan,<sup>†,§</sup> Taegy Shin,<sup>‡</sup> and Baikseok Seong<sup>‡</sup>

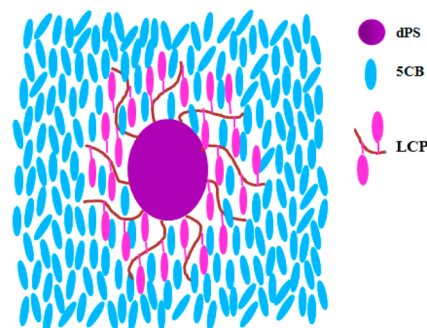
<sup>†</sup>Department of Polymer Science, Kyungpook National University, #1370 Sangyuk-dong, Buk-gu, Daegu 702-701, South Korea

<sup>‡</sup>Neutron Science Division, Korea Atomic Energy Research Institute, 1045 Daedeok-daero, Yuseong-gu Daejeon, 305-353, South Korea

<sup>§</sup>Department of Chemistry, Abdul Wali Khan University, Mardan, 23200 Khyber Pakhtunkhwa, Pakistan

**ABSTRACT:** A diblock copolymer dPS(9.1K)-*b*-LCP(7.2K), the number in parentheses represents the number-averaged molecular weight) with a deuterated polystyrene (dPS) block connected to a side group liquid crystal polymer [poly(6-(4'-cyanobiphenyloxy)hexyl acrylate, LCP)] was self-assembled into  $\sim 78$  Å spherical micelles with a dPS core and LCP corona in a small-molecule nematic liquid crystal solvent, 4-pentyl-4'-cyanobiphenyl (5CB). The micellar structures were examined by small angle neutron scattering (SANS) at various block copolymer concentrations and temperatures. The SANS data was analyzed further using a curve fitting method. The critical micelle concentration (CMC) was as low as  $\sim 0.0027$  wt % and the self-assembled micelles were dissociated reversibly into a unimer state at 33 °C, which is lower than the nematic to isotropic transition temperature ( $T_{ni}$ ) of 5CB (36 °C). The entropic penalty imposed on the dPS by the ordered nematic state of the LC solvent caused phase separation of the flexible dPS block to form micelles and vanished above the  $T_{ni}$  of the LC solvent. A low CMC of  $\sim 0.0027$  wt % suggests that 5CB was a strong selective solvent for dPS-*b*-LCP in the nematic state. The global orientation of 5CB, produced by a magnetic field (MF, 1.2 T) revealed the structure of the dPS core of the micelle to be prolate (elongated sphere) oriented with the long axis along the applied MF direction.

dPS-*b*-LCP micelle in 5CB under magnetic field



## INTRODUCTION

The molecules of liquid crystals (LCs) tend to orient cooperatively in a preferred direction giving rise to useful properties, such as high birefringence, excellent dielectric anisotropy and orientation elasticity, which are forbidden by symmetry in isotropic liquids. The coupling of order with fluidity makes LCs particularly intriguing materials because their orientation-dependent properties can be influenced by readily accessible fields. For example, LCs has many uses in LC displays, which rely on the optical properties of certain liquid crystalline substances in the presence or absence of an electric field. Block copolymers (BCPs) have also attracted considerable attention over the more traditional low molecular weight lipids and surfactants in terms of the enhanced stability and design flexibility, which includes tailoring of the overall molecular weight, architecture and composition.<sup>1</sup> BCPs dissolved in selective solvents (solvents that are good for one block but bad for another) can associate spontaneously to form micelles, with the solvent-insoluble block localized in the micelle core and solvent-soluble block forming a corona (shell) around the core<sup>2</sup> because the insoluble block minimizes contact with the solvent and favors micelle formation. The morphology of the micelles is dependent on a range of variables, such as the block copolymer composition and concentration,<sup>3</sup> type and concentration of the added ions,<sup>4,5</sup>

selectivity of the solvent,<sup>6,7</sup> etc. Among them, the selectivity of the solvent can be defined by the Flory interaction parameter ( $\chi$ ) between the core-forming block and solvent:

$$\chi \approx B + \frac{V_s}{RT}(\delta_p - \delta_s)^2$$

where  $B$  represents the entropic effect (close to 0.34),  $V_s$  is the molar volume of the solvent, and  $\delta_p$  and  $\delta_s$  are the Hansen solubility parameters for the core polymer and solvent, respectively.  $\chi$  can be controlled by changing the solubility parameter and solution temperature. The Eisenberg group screened the effect of solvent selectivity on the micelle structure, and examined poly(styrene-*b*-acrylic acid) (PS-*b*-PAA) ionic diblock copolymers in water/dioxane or water/dimethylformamide mixtures.<sup>8–13</sup> Transitions ranging from spheres, to cylinders, and then to vesicles were observed with increasing the amounts of water in the mixture and hence increasing interfacial tension. Lodge et al. also examined the micelle structures with an asymmetric poly(styrene-*b*-isoprene) (PS(13K)-*b*-PI(71K)) in a series of solvent mixtures including dibutyl phthalate, diethyl phthalate and dimethyl phthalate to

Received: March 7, 2012

Revised: June 9, 2012

Published: July 18, 2012

adjust the degree of solvent selectivity for styrene, and found that the predominant micelle shape changed from spherical to cylindrical, and then to vesicles with increasing solvent selectivity, reflecting the changing interfacial curvature.<sup>13</sup> Our group also studied the micelle structures of poly(styrene-*b*-vinyl4pyridine) (PS-*b*-P4VP) in toluene/ethanol mixtures, which covered PS-selective, neutral, and P4VP-selective solvents.<sup>14–17</sup> Another way to control the solvent selectivity is to change the solvent temperature.  $\chi$  can be controlled by heating (or cooling) the solutions. An increase in solvent temperature will decrease  $\chi$  monotonically for common organic solvents. When the solvent of choice is thermotropic LC molecules, unlike conventional solvents, the phase behavior of a dissolved block copolymer may be ornamented by a discontinuous change in the solvent quality at the LC phase transitions (e.g., a nematic to isotropic phase transition).<sup>18,19</sup> The nematic phase is the simplest of LC mesophases and is characterized by molecules that diffuse freely but tend to retain their orientation in a preferred direction called the director. This orientational order can make LCs in the nematic phase a poor solvent for random coil polymers (e.g., PS) because of the entropic penalty. On the other hand, the two may become completely miscible upon heating to the isotropic phase.<sup>20–22</sup> This random coil polymer can be connected to a LC polymer (LCP) (in a diblock copolymer), which has mesogenic moieties similar to a LC solvent, so that the LCP block is compatible with the LC solvent in both the nematic and isotropic phases due to the absence of an entropic penalty, even in the nematic phase. Therefore, dPS-*b*-LCP may have a structure with dPS in the core and a LCP in the corona in the nematic state of the LC solvent, but a unimer state in its isotropic state. Kornfield et al. examined a high molecular PS(120 K)-*b*-SGLCP(101 K) (SGLCP; side group liquid crystal polymer) in an LC solvent, 4-pentyl-4'-cyanobiphenyl (5CB).<sup>18</sup> They reported that the diblock copolymers had phase-separated into micelles, and 5CB could switch from a strongly selective solvent to a good solvent for the SGLCP block when a nematic to isotropic phase transition occurred. The swelling of a PS-*b*-SGLCP with 5CB enhanced the strength and speed of the response to the electromagnetic stimuli, which makes them promising materials for liquid crystal displays.<sup>1</sup> The magnetic field (MF) effects on the structures in the solution state have rarely been studied. On the other hand, MF induced the alignment of lipid domains in the phospholipid vesicle membranes after reaching the critical size.<sup>23</sup> Moreover, the ordering of LC suspensions of helically twisted rods of cellulose microfibrils under an MF<sup>24</sup> have been reported. A MF (or electric field (EF)) induces the global orientation of LCs, which can control the orientation of the micelle of PS-*b*-LCP if the micelles are anisotropic, such as prolate and oblate. Kornfield et al. also examined the structures of the edge-on and side-on SGLCPs in 5CB using small angle neutron scattering (SANS) under an electrical field, and reported that the type of attachment of LC side groups controlled the chain conformation in such a way that the edge-on and side-on SGLCPs favored oblate and prolate, respectively.<sup>20,25,26</sup> MF alignment of block copolymers has been reported in bulk<sup>27–30</sup> by mixing LC mesogens which were selectively sequestered to one block through hydrogen bonding. A supramolecular complex system formed via hydrogen bond association between poly(acrylic acid) chains and an imidazole-terminated biphenyl mesogen was reported by Gopinadhan et al.<sup>31</sup> They reported that LC mesogens could cocrystallize with the polymer at low temperatures, but function

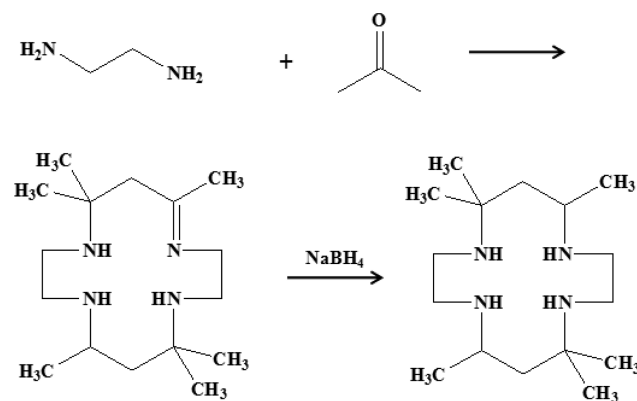
as a solvent at high temperatures. However, the MF alignment of block copolymers with LC mesogens in a nematic liquid crystal solvent has to be considered for exploration.

In this article, a diblock copolymer consisting of a deuterated PS and a liquid crystal polymer (dPS-*b*-LCP) was synthesized using an atom transfer radical polymerization (ATRP) method, and its micellar structures in 5CB solvent were studied using the SANS method at various dPS-*b*-LCP concentrations and solution temperatures. A 1.2 T MF was applied to the LC solutions to view the actual structure of the micelle after aligning the micelle through the induced global orientation of 5CB. The critical micelle concentration (CMC) was measured and the effect of the nematic to isotropic phase transition temperature ( $T_{ni}$ ) on the micelle structure was examined by heating and cooling the solutions. This study provides fundamental information on the formation of micelle structures of flexible chain/LCP diblock copolymers in a nematic LC solvent.

## EXPERIMENTAL SECTION

**Materials.** Deuterated styrene (Sigma-Aldrich) was dried over  $Al_2O_3$  and stored at 4 °C. CuBr was purchased from Sigma-Aldrich and purified over acetic acid. Tetrahydrofuran (THF, Aldrich) was heated with sodium and benzophenone under reflux, and distilled under nitrogen prior to use. All other chemicals were of analytical grade and used as received. The ligand ( $Me_6[14]aneN_4$ ) was made according to Scheme 1. The monomer (6-(4'-cyanobiphenyloxy)hexyl acrylate, LC6) was made according to previous work.<sup>32</sup>

Scheme 1. Synthesis of the Ligand  $Me_6[14]aneN_4$



**Synthesis of  $Me_6[14]aneN_4$ .** The ligand 5,5,7,12,12,14-hexamethyl-1,4,8,11-tetraazamacrocyclotetradecane ( $Me_6[14]aneN_4$ ) was prepared in three steps according to Scheme 1.<sup>33</sup> In the first step, 1,2-diaminoethane dihydrobromide was prepared by adding 1,2-diaminoethane (10 mL, 0.15 mol) in methanol (100 mL). The solution was cooled in an ice bath, and concentrated hydrobromic acid (44%, 34 mL) was added dropwise. The white precipitate was filtered, washed with *n*-butanol followed by ether, and dried in a vacuum oven at room temperature. Acetone (100 mL) and 1,2-diaminoethane (3.0 g, 0.05 mol) were added to 1,2-diaminoethane dihydrobromide (10.0 g, 0.05 mol), and the mixture was stirred and heated to 45 °C for 50 min. During this time, a white precipitate of macrocycle dihydrobromide was formed. The solution was cooled and the product was filtered, washed with acetone followed by ether, and finally dried in a vacuum oven at room temperature for 24 h. In the final step, *trans*-[14]-diene dihydrobromide dehydrate (14.0 g) was dissolved in methanol (180 mL). Subsequently, sodium borohydride (3.0 g) was added in small portions to this warmed solution. The solution was heated in a water-bath until effervescence was complete. A 2 M potassium hydroxide solution was then added until the mixture was

basic (pH 12), and the solution was cooled to room temperature and filtered. Approximately 50% methanol was evaporated off, and the resulting solution was cooled in an ice bath to obtain fine  $\text{Me}_6[14]\text{aneN}_4$  crystals. The product was recrystallized from methanol, filtered off and dried in a vacuum oven at room temperature for 24 h. Figure 1 shows the NMR spectrum of  $\text{Me}_6[14]\text{aneN}_4$ .  $^1\text{H}$  NMR

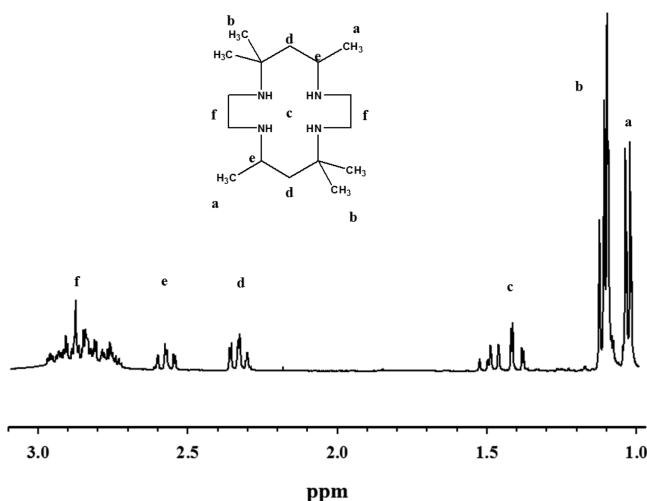


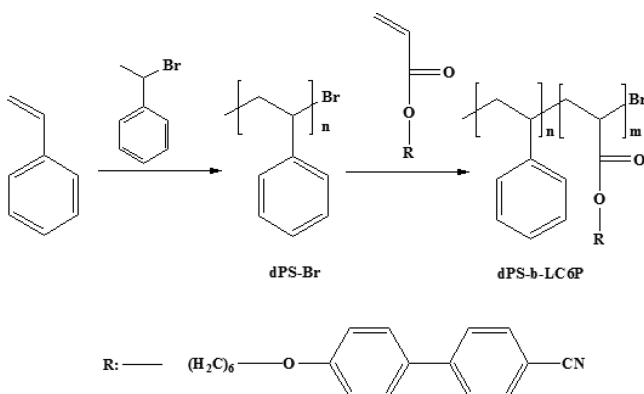
Figure 1.  $^1\text{H}$  NMR spectrum of  $\text{Me}_6[14]\text{aneN}_4$ .

( $\text{CDCl}_3$ , 400 MHz, 298 K) peaks were observed at  $\delta = 2.7\text{--}2.9$  (m, 8H,  $(\text{CH}_2)_4$ ), 2.58 (td, 2H,  $(\text{CH}_2)_2$ ), 2.3 (m, 4H,  $(\text{CH}_2)_2$ ), 1.56–1.38 (m, 4H,  $(\text{NH})_4$ ), 1.18 (m, 12H,  $(\text{CH}_3)_4$ ), and 0.99 (d, 6H,  $(\text{CH}_3)_2$ ).

**Synthesis of a dPS–Br Macroinitiator.** CuBr (68.88 mg, 0.48 mmol) was placed in a Schlenk flask and dried under vacuum. 1-bromoethylbenzene (1-PEBr, initiator) (0.068 mL, 0.48 mmol), deuterated styrene monomer (7.01 mL, 66.5 mmol), and  $N,N,N,N,N$ -pentamethyl diethylenetriamine (PMDETA, ligand) were combined in a tube and degassed (by bubbling nitrogen through it for 60 min). They were then introduced into the flask with a syringe that had been purged with dry nitrogen. The flask was then placed in a 110 °C oil bath and stirred for 2 h. The resulting polymer solution was poured into a large volume of methanol. The dPS homopolymer (dPS–Br) obtained was purified by reprecipitating three times in a THF/methanol system to remove the unreacted monomers, CuBr and PMDETA. The polymer was then dried under vacuum at 40 °C for 24 h, giving a yield of 67%. The polymer had a number-average molecular weight ( $M_n$ ) of  $9.1 \times 10^3$  with a polydispersity index (PDI,  $M_w/M_n$ ) of 1.09.

**Synthesis of a dPS–*b*-LCP.** Scheme 2 shows a schematic diagram of the synthesis of a dPS–*b*-LCP. In a typical procedure, the monomer (LC6, 350 mg, 1 mmol), CuBr (1.76 mg, 0.013 mmol),  $\text{Me}_6[14]\text{aneN}_4$

Scheme 2. Schematic of the Synthesis of dPS–*b*-LCP



(10.24 mg, 0.037 mmol, ligand) and dPS–Br (9.1K, 127.30 mg, 0.012 mmol) were placed into a Schlenk flask and dried under vacuum. Anisole (0.72 mL), which had previously been degassed by bubbling with nitrogen, was then introduced into the flask using a syringe. The flask was then heated in an oil bath at 80 °C for 64 h. The dPS–*b*-LCP obtained was purified by precipitating three times in methanol to remove the unreacted monomers and dried under vacuum at 40 °C for 24 h. The yield calculated gravimetrically was 60%.

**Characterization.** The molar masses and molar mass distributions were determined by gel permeation chromatography (GPC) with a PL GEL Organic GPC Column and RI750F refractive index detector (Young Lin Instrument Co., Acme 9000, Korea). THF was used as the eluent with a flow rate of 1.0 mL/min and calibration was carried out with polystyrene standards (Aldrich Chemical Co., USA). Fourier Transform Infrared (FT–IR) spectroscopy of dPS–*b*-LCP was performed using a Jasco FT/IR–620 FT-IR spectrometer.  $^1\text{H}$  nuclear magnetic resonance (NMR) spectroscopy of dPS–*b*-LCP and  $\text{Me}_6[14]\text{aneN}_4$  was performed at ambient temperature using a 400 MHz Bruker spectrometer with deuterated chloroform ( $\text{CDCl}_3$ ) as a solvent. The SANS measurements were carried out on a HANARO SANS instrument at the Korea Atomic Energy Research Institute (KAERI) in Daejeon, Korea. The solution was filled into a quartz cell with a 2 mm neutron path length. The wavelength ( $\lambda$ ) was 6.38 Å with a full width at half-maximum,  $\Delta\lambda/\lambda = 0.1$ . A sample to detector distance of 1.8 m was used to cover a  $q$  range of 0.004–0.04 Å $^{-1}$ , where  $q = (4\pi/\lambda) \sin \theta/2$  is the magnitude of the scattering vector with  $\theta$  being the scattering angle. The scattered neutrons were collected on a two-dimensional (2D) area detector and circularly averaged. In the case of the MF experiment, the patterns were scanned at the selected regions (either horizontally or vertically) with an azimuthal angle span of 30° at the centers of the horizontal and vertical directions. Sample scattering was corrected for the background, empty cell scattering and sensitivity of the detector. To explore the effect of the global orientation of the LC solvent on the micelle structure in the LC solvent, SANS measurements under a MF of 1.2 T was carried out at room temperature. MF was applied horizontally in vertical direction to the neutron beam. Samples were placed in a holder of a specially designed aluminum stage within a magnet (Walker Scientific Inc.) at a flux density of 1.2 T.

**SANS Data Analysis.** The neutron scattering length densities of the 5CB and LCP block in dPS–*b*-LCP were similar and dPS exhibited stronger scattering than those of the LCP and 5CB in the neutron beam. Therefore, the resulting scattering profiles from the sample mainly reflect the size and shape of the dPS core. The core of the micelle was fitted with the form factor of the spheres with a Gaussian size distribution. The normalized Gaussian distribution is given by the following equation:

$$f(R) = \frac{1}{\sigma\sqrt{2\pi}} \exp\left[-\frac{1}{2\sigma^2}(R - R_{\text{avg}})^2\right] \quad (1)$$

where  $R_{\text{avg}}$  is the mean radius, and  $\sigma$  is the standard deviation from which the polydispersity ( $p$ ) can be calculated by  $\sigma/R_{\text{avg}}$ . For a sphere with radius  $R$ , the scattering amplitude  $F(q,R)$  is given by the following equation:

$$F(q, R) = \frac{3[\sin(qR) - qR \cos(qR)]}{(qR)^3} \quad (2)$$

The total scattering intensity can be expressed as

$$I(q) = \left(\frac{4\pi}{3}\right)^2 N_0 \Delta\rho^2 \int_0^\infty f(R) R^6 F^2(q, R) dR + I_{\text{BKG}} \quad (3)$$

where  $N_0$  is the total number of particles per unit volume with  $N_0 = \Phi/\langle V \rangle$ ,  $\Phi$  is the volume fraction,  $\langle V \rangle$  is the mean volume of a particle,  $\Delta\rho$  is the difference in the scattering length density, and  $I_{\text{BKG}}$  is the background due to incoherent scattering from protons. The parameters of the form factor,  $\Phi$ ,  $p$ , scattering length density of the sphere, scattering length density of the solvent, and incoherent background were obtained using the curve fitting function of IgorPRO.

The micelle aggregation number was calculated using the formula,  $N_{agg} = V_m/v_{dPS}$ , where the micelle volume was calculated using  $V_m = (4\pi/3)R^3$  and the volume of the dPS molecule  $v_{dPS}$  ( $1.43886 \times 10^4 \text{ \AA}^3$ ) was derived from the density of dPS of  $1.05 \text{ g/cm}^3$  and molecular weight of dPS of 9100.

## RESULTS AND DISCUSSION

**Synthesis of dPS-*b*-LCP.** The dPS-*b*-LCP obtained had an  $M_n$  of 16.3 K with a PDI of 1.21, which means that

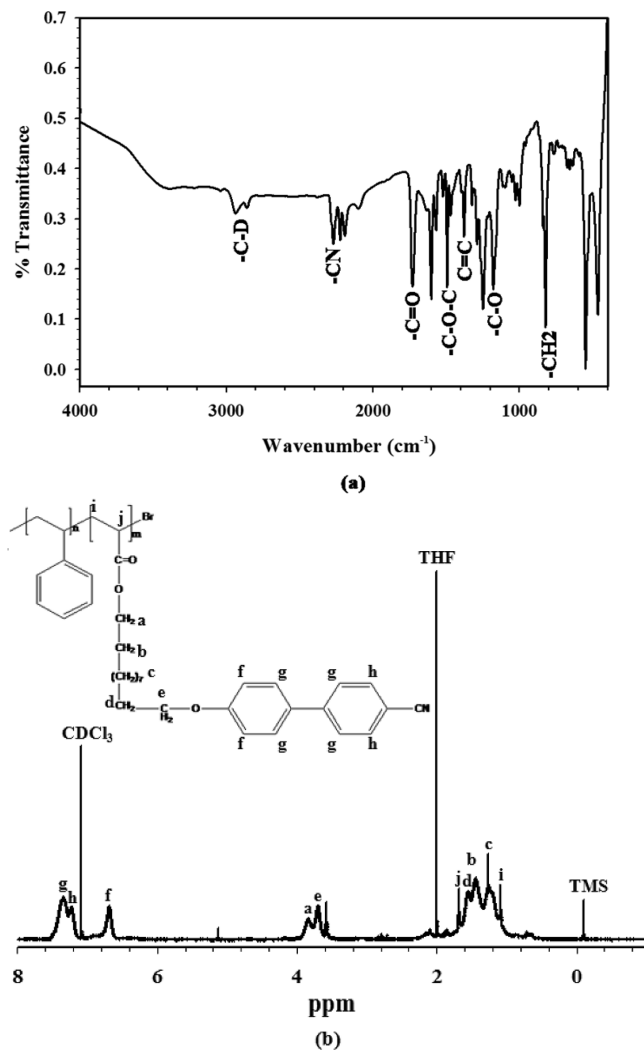


**Figure 2.** (a) FT-IR and (b)  $^1\text{H}$  NMR spectra of dPS-*b*-LCP.

approximately 7.2 K of the LC6 monomer units ( $\sim 21$  monomer units) were attached to 9.1 K of the dPS macroinitiator, even though this molecular weight is relative to the standard PS. Figure 2a shows the FT-IR spectrum of dPS-*b*-LCP. The  $-\text{C}-\text{D}$  stretching bands of dPS were observed at approximately  $2942 \text{ cm}^{-1}$ . The  $-\text{C}-\text{H}$  stretching normally occurs at approximately  $3000$  to  $3100 \text{ cm}^{-1}$  but when H is substituted with D, the increase in mass from the attached D atom causes absorption at a lower frequency. The peaks at  $2290$ ,  $1750$ ,  $1500$ ,  $1400$ , and  $1113 \text{ cm}^{-1}$  correspond to the stretching bands of the CN, C=O,  $\text{C}_{\text{aliphatic}}-\text{O}-\text{C}_{\text{aromatic}}$ , aromatic C=C, and C-O groups of LCP, respectively. The peak at  $827 \text{ cm}^{-1}$  represents the long aliphatic  $\text{CH}_2$  in the spacer of the LCP. Therefore, the existence of functional groups in both blocks in the FT-IR spectrum indicates

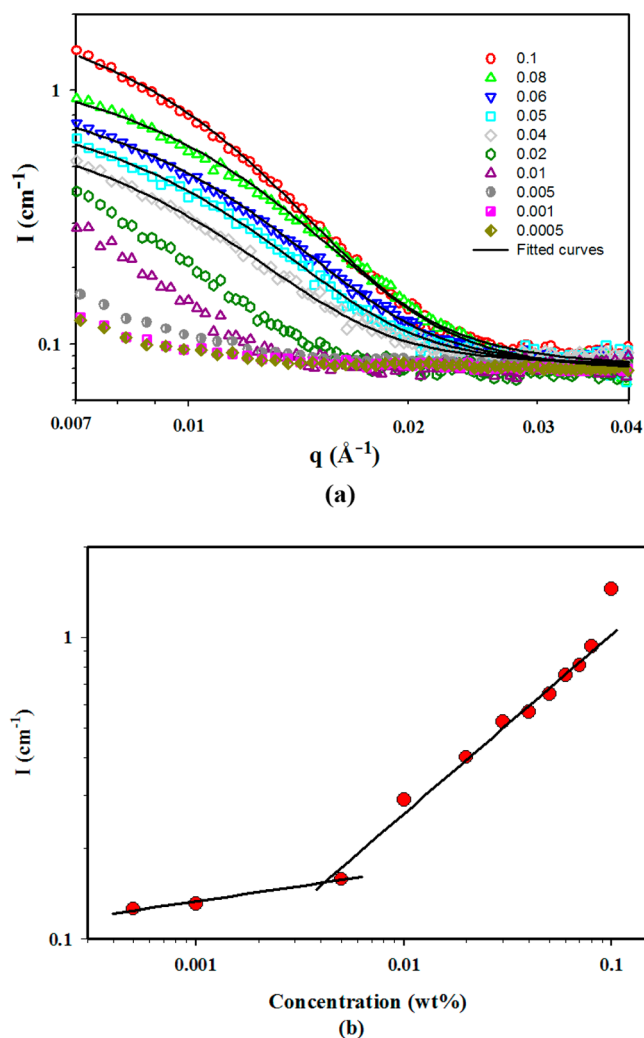


**Figure 3.** (a) Experimental (symbols) and curve-fitted (lines) SANS patterns of the dPS-*b*-LCP solutions in 5CB with different concentrations at  $25 \text{ }^\circ\text{C}$ , and (b) the plot of the intensities at  $q = 0.007 \text{ \AA}^{-1}$  against the solution concentrations; the numbers in (a) are the concentration of dPS-*b*-LCP in wt %.

**Table 1.** Structural Parameters of the Micelle Obtained from Curve Fitting of the SANS Data at Various Concentrations

concentration (wt %)	$R$ ( $\text{\AA}$ )	spherical	
		$p$ ( $\sigma/R_{\text{avg}}$ )	$N_{\text{agg}}$
0.1	$83.36 \pm 0.30$	$0.913 \pm 0.003$	153
0.08	$73.62 \pm 0.20$	$0.903 \pm 0.003$	105
0.07	$83.04 \pm 0.42$	$0.949 \pm 0.006$	167
0.06	$76.69 \pm 0.34$	$0.901 \pm 0.005$	119
0.05	$80.11 \pm 0.32$	$0.882 \pm 0.005$	136
0.04	$78.88 \pm 0.73$	$0.991 \pm 0.012$	130

successful block copolymerization. Figure 2b shows the NMR spectrum of dPS-*b*-LCP. The  $^1\text{H}$  NMR spectrum exhibited proton peaks of the main chain backbone of  $\text{CH}_2-\text{CH}$  in the LCP at 1.68 and 1.11 ppm, which had shifted from the normal vinyl group positions of the monomer due to polymerization.<sup>34</sup> The spectrum showed signals at 1.26, 1.45, 1.56, 3.74, and 3.85 ppm, which corresponded to the  $\text{CH}_2$  spacer in the LCP block. The doublets at 7.36 and 7.26 ppm and the singlet at 6.68 ppm were assigned to the protons from the benzene ring of the

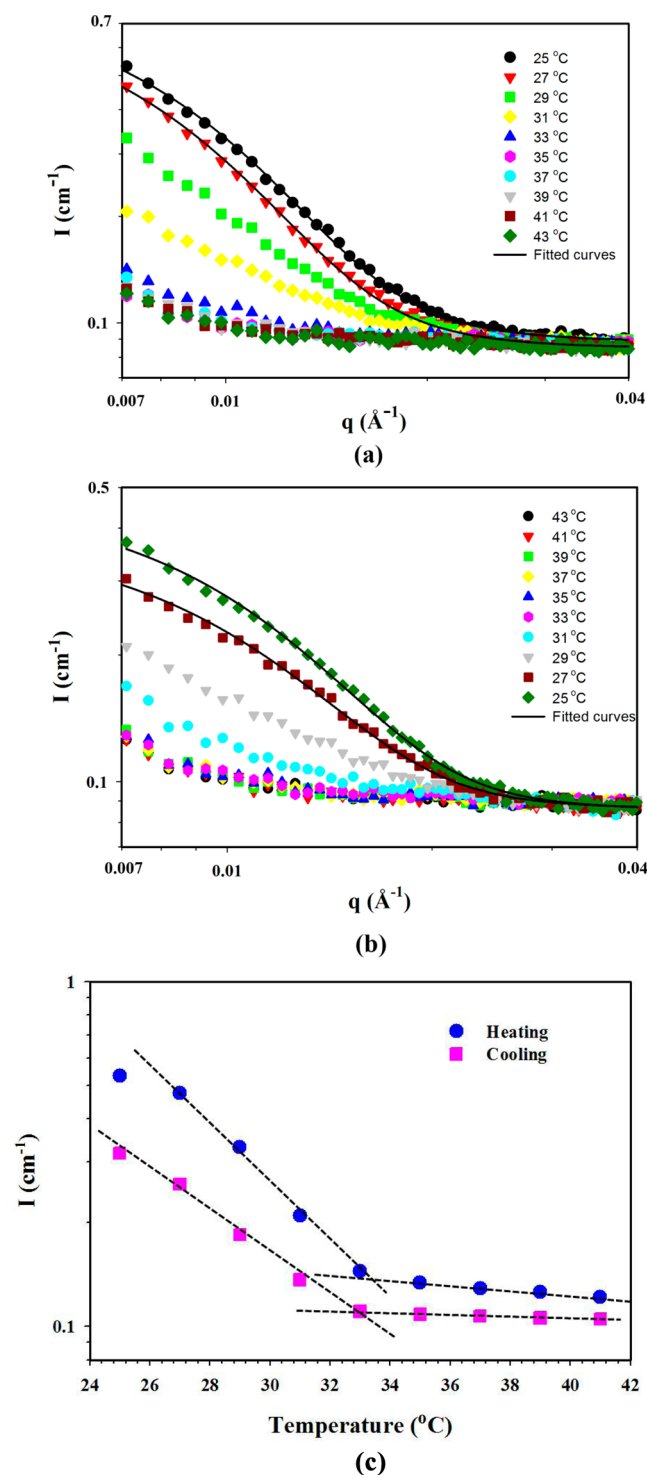


**Figure 4.** SANS patterns of a 0.2 wt % dPS-*b*-LCP solution in 5CB at different temperatures during (a) heating and (b) cooling and (c) the plot of their intensities at  $q = 0.0071$  Å<sup>-1</sup>.

biphenyl ring of the LCP. The peak at 2 ppm was assigned to THF, the dissolving solvent.

To produce micelles in 5CB, dPS-*b*-LCP and 5CB were dissolved together in dichloromethane (DCM) followed by stirring and heating at 40 °C overnight to remove the DCM. Figure 3 shows the SANS patterns from 0.1, 0.08, 0.07, 0.06, 0.05, 0.04, 0.02, 0.01, 0.005, 0.001, and 0.0005 wt % dPS-*b*-LCP solutions in 5CB at room temperature. The initial scattering

with high intensity decreased significantly with increasing  $q$  and merged at  $q > \sim 0.025$  Å<sup>-1</sup>. The strong SANS scattering indicated that micelle structures of dPS-*b*-LCP had formed in the nematic state of the LC solvent, and detailed structures were determined by analyzing the SANS curves.

A close inspection of the scattering patterns at various solution concentrations ( $c$ s) revealed a decrease in magnitude of the scattered intensity at a low  $q$  value with decreasing  $c$  until 0.005 wt %. The SANS patterns at  $c = 0.005$ , 0.001, and 0.0005 wt % were similar to each other indicating that micelles had not formed at these low concentrations and the block copolymers were in a unimer state. Figure 3b shows the intensities of SANS patterns at  $q = 0.007$  Å<sup>-1</sup> as a function of  $c$ . Two lines representing a constant and increasing intensity were drawn. The concentration at the crossover point of the two straight lines, 0.0027 wt %, was the CMC. This low CMC indicates that 5CB is a strong selective solvent for dPS-*b*-LCP in the nematic state.

Table 1 lists the radii of the micelle core,  $R$ , with  $p$  ( $\sigma/R_{\text{avg}}$ ) and micelle aggregation number,  $N_{\text{agg}}$  with respect to  $c$ , which was calculated using a curve fitting method (Figure 3c) assuming a spherical shape for the micelle core and a Gaussian normal size distribution. The curve fit was possible until  $c = 0.04$  wt % because the scattering intensities at  $c < 0.04$  wt % were too low and scattered to obtain a good fit. The  $R$  and  $N_{\text{agg}}$  of all the solutions studied were in the ranges 76–83 Å and 105–167, respectively. This independence might be due to the strong selectivity of 5CB to dPS-*b*-LCP. On the other hand, SANS scattering at  $c < 0.04$  wt % might show their dependency on  $c$ , even though they require more resolution to analyze them. From analysis of chain dimensions, the chain length of the most extended and random-coil chains of dPS(9.1K) in the unperturbed state (as the solvent is extremely poor for the dPS chains) were 109 and 45 Å, respectively, where the chain length of the random-coil chains were calculated using  $r^2 = n^2 C_{\infty}$ , where  $C_{\infty} = 9.85$ .<sup>35</sup> The  $R$  value of  $\sim 80$  Å from SANS was higher than the length of the random-coil chain and close to that of the most extended chain so that there is considerable space between the dPS chains in the core. This space might be filled with 5CB so that the real aggregation number would be lower than the values listed in Table 1. The interfacial area between the core and corona of the micelle is 804 nm<sup>2</sup> for a micelle with an 8 nm radius. The interfacial area occupied by a chain ( $a$ ) would be 6 nm<sup>2</sup> (804 nm<sup>2</sup> /  $\sim 136$  chains), which is slightly lower than the value reported for a PS-*b*-PI spherical micelle (13 nm<sup>2</sup>).<sup>13</sup> This decrease of  $a$  as compared to that of the PS-*b*-PI micelle might be due to the SCBs incorporated in the dPS core, which would reduce  $N_{\text{agg}}$  and increase  $a$ . The sizes of the micelle core of PS(13K)-*b*-PI(71K) in di-*n*-butyl phthalate (DBP)/ diethyl phthalate (DEP) and PS(9.1K)-*b*-LCP(7.2K) in 5CB were 29 and 8 nm, respectively. The size of core of the PS(9.1K)-*b*-LCP(7.2K) micelle in 5CB was smaller than that of the PS(13K)-*b*-PI(71K) micelle in DBP/DEP due to the short chain length. However, even though the short chain length of PS(9.1K)-*b*-LCP(7.2K) were considered, the micelle size of PS(9.1K)-*b*-LCP(7.2K) micelle in 5CB was smaller than of PS(13K)-*b*-PI(71K) in DBP/DEP because the molecular weight decreased by a factor of 30% but the size decreased by a factor of 68%. This large decrease in micelle size might be due to the less selectivity of 5CB than DBP/DEP toward PS so that 5CB might easily penetrate into the dPS core.

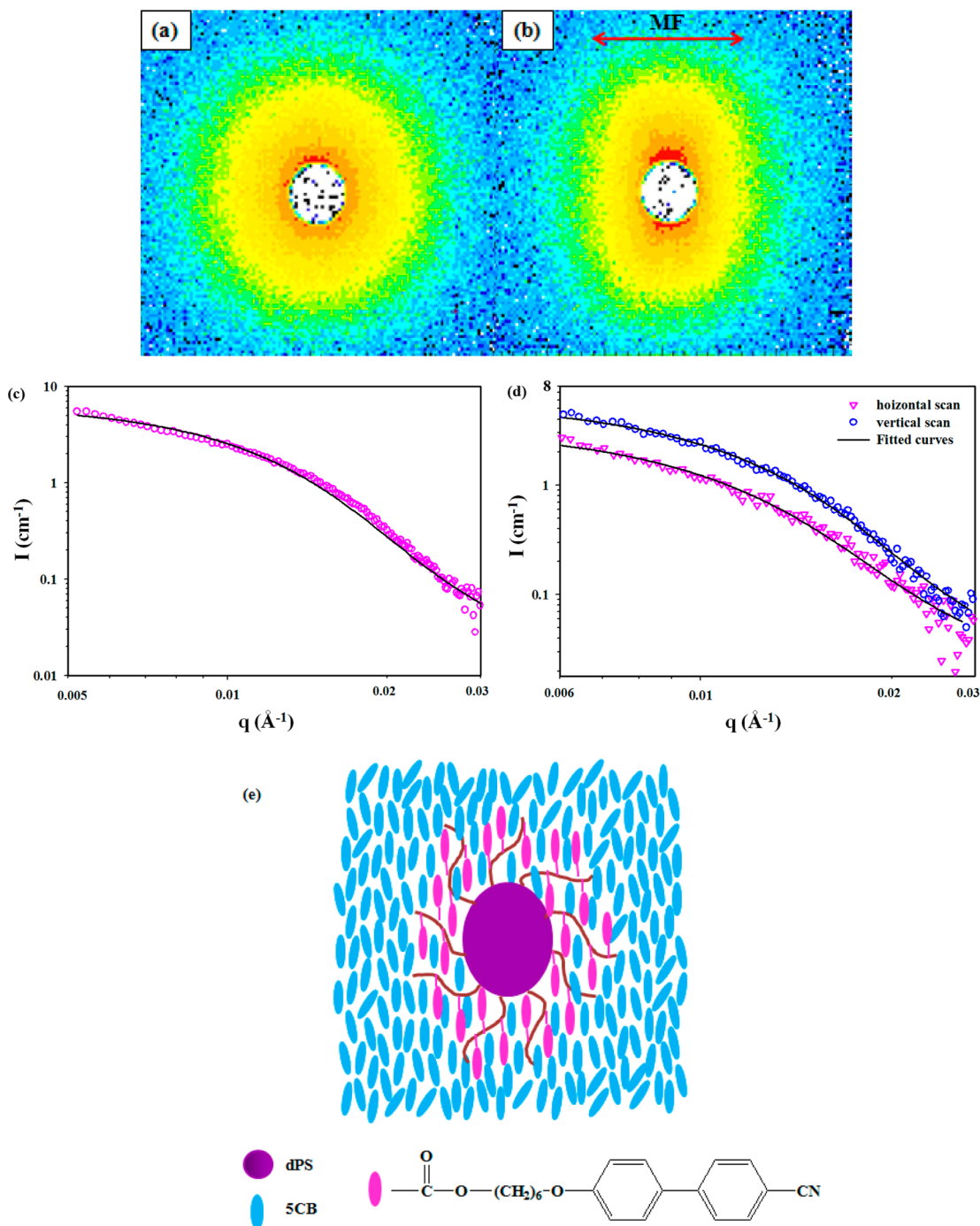


**Figure 5.** 2D SANS patterns of a 0.2 wt % dPS-*b*-LCP solution in 5CB at room temperature (a) without MF and (b) with MF of 1.2 T; (c) azimuthally averaged 1D scanned data of (a); (d) azimuthally averaged 1D scanned data of part b along the MF direction and perpendicular to it with an averaged azimuthal angle of 30°; (e) schematic diagram of the micelle structure in 5CB under MF which direction is vertical.

Figure 4 shows the evolution of a SANS patterns of a 0.2 wt % dPS-*b*-LCP solution in 5CB during heating and cooling over the temperature range between 25 and 43 °C with an increase (or decrease) of 2 °C along with a plot of their intensities at  $q = 0.0071 \text{ \AA}^{-1}$  as a function of temperature. The changes in the scattering patterns during heating and cooling were similar, indicating that the structure formation is reversible. At temperatures above the  $T_{ni}$  of 5CB (36 °C), the scattered intensity was low and constant, suggesting that the micelle structure had not formed and the block copolymers were in the unimer state. At temperatures lower than the  $T_{ni}$  of 5CB, the

scattered intensity began to increase with decreasing temperature due to micelle formation.

The plot of the intensities at  $q = 0.0071 \text{ \AA}^{-1}$  against temperature clearly (Figures 4c) demonstrated the isotropic state of the solution at temperatures higher than the  $T_{ni}$  of 5CB and micelle formation at temperatures lower than the  $T_{ni}$  of 5CB. The scattering angle at  $q = 0.007 \text{ \AA}^{-1}$  has been chosen because it is close to the lowest angle which could be measurable;  $I(q = 0)$  represents the total scattering so that the data at low angles might be more reliable and less scattered. The temperature at which the micelle structures had formed

( $T_{\text{micelle}}$ ) was acquired from the intercept of the horizontal line and the tangent line in the region of the increasing intensity. The intercepting temperatures for heating and cooling were 33.2 and 33.1 °C, respectively. These  $T_{\text{micelle}}$ s were lower than the  $T_{\text{ni}}$  of pure 5CB (~36 °C). The block copolymers might play as impurities which could cause the decreased  $T_{\text{ni}}$ . However, we could not find any change of the  $T_{\text{ni}}$ . The lower  $T_{\text{micelle}}$  than that of  $T_{\text{ni}}$  might be due to the 5CBs incorporated in the dPS core, which might cause easier dissociation of the micelles. Similar phenomena were observed by the Kornfield group<sup>26</sup> for PS-*b*-SGLCPs with a short PS block length. The values of the  $R$  (and  $N_{\text{agg}}$ ) decreased from  $74.92 \pm 10.18 \text{ \AA}$  (and 132) to  $69.83 \pm 9.04 \text{ \AA}$  (and 94) as temperature increased from 25 to 27 °C. The curve fit was possible at 25 and 27 °C because the scattering intensities at higher than 27 °C were too low and scattered to obtain a good fit. The intensities in Figure 4c also decreased continuously as temperature increased until  $T_{\text{micelle}}$ . These results indicate that the selectivity of the 5CB continuously decreased as temperature increased (not a discrete way at  $T_{\text{micelle}}$ ) even though the temperatures were still below  $T_{\text{micelle}}$ . The incorporated 5CB in the dPS core might play as a mixed solvent and lose the liquid crystal properties so that the selectivity of the 5CB continuously decreased leading to the decreased intensity,  $R$  and  $N_{\text{agg}}$  as temperature increased.

To examine the anisotropic micellar structure, a 1.2 T MF was applied to the LC solution at room temperature to obtain the global orientation of the LC solvent during the SANS measurements. The spherical micelle would show isotropic SANS scattering even at the global orientation of the LC, even though the anisotropic micelle (such as prolate and oblate) exhibits anisotropic SANS scattering when it is aligned along the direction of the global orientation of the LC. This alignment can occur due to the mesogenic groups in the corona, which anchor 5CB strongly. Figure 5 shows the 2D patterns and azimuthally averaged 1D scanned data with and without a MF. The azimuthally averaged 1D scanned data with the MF were obtained by azimuthal averaging of 30° along the horizontal and vertical directions. The 2D SANS pattern was isotropic in the absence of MF (Figure 5a), indicating randomly oriented liquid crystal domains. Curve fitting of the 1D SANS pattern (Figure 5c) yielded a radius of 78 Å. An ellipsoidal pattern was observed with their long axis in the vertical direction when a 1.2 T MF was applied along the horizontal direction (Figure 5b), indicating that the dPS core had a prolate shape possibly due to the end-on attachment of mesogenic groups, as depicted in Figure 5e. The long and short axes of the ellipse were estimated by fitting the 1D scattering curve of vertically and horizontally scanned 2D data (Figure 5d) with the form factor of a sphere. The resulting values for the long and short axes are 105.7 and 75.5 Å, respectively.

## CONCLUSION

The micelle structures of dPS-*b*-LCP in the 5CB solvent were examined as functions of the block copolymer concentration and temperature using SANS. MF was applied to determine the anisotropic structure of a micelle through the global orientation of the LC. Micelles of the dPS-*b*-LCP formed reversibly in the nematic state of the 5CB, even though the temperature at which the micelle had formed was 3 °C lower than its  $T_{\text{ni}}$ . The CMC was as low as ~0.0027 wt %, indicating the strong selectivity of the nematic state of 5CB to dPS-*b*-LCP. The applied MF revealed the prolate structure of the micelle core,

which was attributed to the end-on type of attachment of the mesogenic groups in the LCP block.

## AUTHOR INFORMATION

### Corresponding Author

\*E-mail: psy@knu.ac.kr.

### Notes

The authors declare no competing financial interest.

## ACKNOWLEDGMENTS

This work was supported by the National Research Foundation of Korea (NRF-2011-0020264, and NRF-2009-0073476).

## REFERENCES

- (1) Lodge, T. P.; Bang, J. A.; Li, Z. B.; Hillmyer, M. A.; Talmon, Y. *Faraday Discuss.* **2005**, *128*, 1–12.
- (2) Alexandridis, P.; Spontak, R. J. *Curr. Opin. Colloid Interface Sci.* **1999**, *4* (2), 130–139.
- (3) Eisenberg, L. Z. a. A. *Science* **1995**, *268*, 4.
- (4) Lifeng Zhang, A. E. *Macromolecules* **1996**, *29* (27), 10.
- (5) van der Maarel, J. R. C.; Groenewegen, W.; Egelhaaf, S. U.; Laap, A. *Langmuir* **2000**, *16* (19), 7510–7519.
- (6) Eisenberg, Y. Y. a. A. *J. Am. Chem. Soc.* **1997**, *119* (35), 8383–8384.
- (7) Ding, J. F.; Liu, G. J. *Macromolecules* **1999**, *32* (25), 8413–8420.
- (8) Shen, H. W.; Eisenberg, A. *J. Phys. Chem. B* **1999**, *103* (44), 9473–9487.
- (9) Chen, L.; Shen, H. W.; Eisenberg, A. *J. Phys. Chem. B* **1999**, *103* (44), 9488–9497.
- (10) Zhang, L. F.; Eisenberg, A. *Macromolecules* **1999**, *32* (7), 2239–2249.
- (11) Shen, H. W.; Eisenberg, A. *Macromolecules* **2000**, *33* (7), 2561–2572.
- (12) Choucair, A.; Eisenberg, A. *Eur. Phys. J. E* **2003**, *10* (1), 37–44.
- (13) Bang, J.; Jain, S. M.; Li, Z. B.; Lodge, T. P.; Pedersen, J. S.; Kesselman, E.; Talmon, Y. *Macromolecules* **2006**, *39* (3), 1199–1208.
- (14) Ali, N.; Park, S. Y. *Langmuir* **2008**, *24* (17), 9279–9285.
- (15) Park, S. Y.; Sul, W. H. *Polymer* **2008**, *49* (15), 3327–3334.
- (16) Park, S. Y.; Chang, Y. J.; Farmer, B. L. *Langmuir* **2006**, *22* (26), 11369–11375.
- (17) Park, S. Y.; Sul, W. H.; Chang, Y. J. *Macromolecules* **2007**, *40* (10), 3757–3764.
- (18) Fischer, H.; Poser, S. *Acta Polym.* **1996**, *47* (10), 413–428.
- (19) Wong, G. C. L.; Commandeur, J.; Fischer, H.; Jeu, W. H. d. *Phys. Rev. Lett.* **1996**, *77* (26), 5221–5224.
- (20) Scruggs, N. R.; Kornfield, J. A.; Lal, J. *Macromolecules* **2006**, *39* (11), 3921–3926.
- (21) Benmouna, F.; Daoudi, A.; Roussel, F.; Buisine, J. M.; Coqueret, X.; Maschke, U. *J. Polym. Sci., Part B: Polym. Phys.* **1999**, *37* (15), 1841–1848.
- (22) Gogibus, N.; Maschke, U.; Benmouna, F.; Ewen, B.; Coqueret, X.; Benmouna, M. *J. Polym. Sci., Part B: Polym. Phys.* **2001**, *39* (5), 581–588.
- (23) Beck, P.; Liebi, M.; Kohlbrecher, J.; Ishikawa, T.; Ruegger, H.; Zepik, H.; Fischer, P.; Walde, P.; Windhab, E. *J. Phys. Chem. B* **2010**, *114* (1), 174–186.
- (24) Orts, W. J.; Godbout, L.; Marchessault, R. H.; Revol, J. F. *Macromolecules* **1998**, *31* (17), 5717–5725.
- (25) Kempe, M. D.; Scruggs, N. R.; Verduzco, R.; Lal, J.; Kornfield, J. A. *Nat. Mater.* **2004**, *3* (3), 177–182.
- (26) Scruggs, N. R.; Verduzco, R.; Uhrig, D.; Khan, W.; Park, S. Y.; Lal, J.; Kornfield, J. A. *Macromolecules* **2009**, *42* (1), 299–307.
- (27) Majewski, P. W.; Gopinadhan, M.; Jang, W. S.; Lutkenhaus, J. L.; Osuji, C. O. *J. Am. Chem. Soc.* **2010**, *132* (49), 17516–17522.
- (28) Majewski, P. W.; Gopinadhan, M.; Osuji, C. O. *J. Polym. Sci., Part B: Polym. Phys.* **2012**, *50* (1), 2–8.

- (29) Gopinadhan, M.; Majewski, P. W.; Beach, E. S.; Osuji, C. O. *ACS Macro Lett.* **2012**, *1* (1), 184–189.
- (30) Gopinadhan, M.; Majewski, P. W.; Osuji, C. O. *Macromolecules* **2010**, *43* (7), 3286–3293.
- (31) Gopinadhan, M.; Beach, E. S.; Anastas, P. T.; Osuji, C. O. *Macromolecules* **2010**, *43* (16), 6646–6654.
- (32) Lee, D. Y.; Seo, J. M.; Khan, W.; Kornfield, J. A.; Kurji, Z.; Park, S. Y. *Soft Matter* **2010**, *6* (9), 1964–1970.
- (33) Bodie, E. *Inorganic Synthesis*; John Wiley: New York, 1978; Vol. 18.
- (34) Khan, W.; Seo, J. M.; Park, S. Y. *Soft Matter* **2011**, *7* (2), 780–787.
- (35) Sperling, L. H. *Introduction to Physical Polymer Science*, 3rd ed.; Wiley: New York, 2001; p 178.